

Petrogenesis and Sr-Nd isotope Geochemistry of Neogene Igneous Rocks in the Goloumak Area, South of Kerman, Iran

F. Arzhangnezhad¹, Gh. R. Ghadami^{2*}, M. Poosti³, M. Fadaeian⁴

¹ Department of Geology, University of Hormozgan, Bandar Abbas, Hormozgan, Islamic Republic of Iran

² Department of Geology, University of Hormozgan, Bandar Abbas, Hormozgan, Islamic Republic of Iran

³ Department of Geology, University of Hormozgan, Bandar Abbas, Hormozgan, Islamic Republic of Iran

⁴ Department of Geology, Payame Noor University, Tehran, Islamic Republic of Iran

Received: 20 June 2023 / Revised: 22 Decemver 2023 / Accepted: 3 February 2024

Abstract

The study area is near Goloumak village, 30 km south of Kerman. These rock units consist of acidic rhyolite and dacite, as well as intermediate andesite, basalt, and trachyandesite. Mafic igneous rocks are alkaline, and intermediate rocks are calc-alkaline to transition range. Volcanic rocks exhibit depletion in Ba, Ti, Nb, and Ta, as well as enrichment in K, Rb, and Th. Basaltic rocks were formed by partial melting of the mantle, based on $^{87}\text{Sr}/^{86}\text{Sr}$ and $^{144}\text{Nd}/^{143}\text{Nd}$ isotopic ratios. Samples show relative enrichment of $^{87}\text{Sr}/^{86}\text{Sr}$ in the mantle array on the Sr-Nd isotope correlation diagram. Mafic rocks are affected by subduction of lithospheric slab or mantle crust metasomatism, as per the comparison of studied samples in the $^{143}\text{Nd}/^{144}\text{Nd}$ isotope correlation diagram versus $^{87}\text{Sr}/^{86}\text{Sr}$. Based on Sr-Nd geochronological data, the rocks were formed at 12.5 ± 2.0 Ma, corresponding to the Miocene for the basaltic rocks. All samples are in a continental arc margin and post-collision volcanic arc. The magma source is from low to intermediate partial melting of the mantle, as indicated by the LREE/HREE ratio of the mafic and intermediate rocks. LREE enrichment is due to low partial melting of mantle source and magma contamination by crust materials. Basalts show a low melting degree of the mantle for magma formation. Depletion of these rocks of HREE in the source shows garnet in genesis. La and Sm abundance in the studied composition is similar to magma derived from the enriched mantle, comprising about 1-5% of lherzolitic garnet.

Keywords: Petrogenesis; Sr-Nd Isotope; Neogene; Goloumak; Kerman.

Introduction

The Central Iran Zone is one of the most prominent

regions in Iran. This zone has been the scene of the oldest metamorphism (Precambrian) and the youngest active volcanism (1, 2). Various geological processes

* Corresponding Author: Tel: 09178395240; Email: ghadami@hormozgan.ac.ir

have taken place in this region, which is the oldest micro-continent plate in Iran (3). The formation of various structural zones in Iran is due to the subduction of Neo-Tethys beneath the Central Iran Microplate (CIM) and the collision of Iranian and Afro-Arabian plates (4). The peak of this subduction-related calc-alkaline magmatic activity has seemingly occurred throughout the Eocene. Most parts of Iran except Koppeh Dagh and Zagros experienced intense volcanic and plutonic activities in the Tertiary, with volcanism climax in the Eocene and intense plutonic in the Oligocene and Miocene (5).

There are two main theories about the tectonic setting of tertiary magmatism in Iran. (6). The first theory for Tertiary magmatism, especially in the Eocene, is due to a thermal plume beneath the Iranian block. According to proponents of this theory, an intercontinental rift has formed. However, it was subsequently closed due to the Pyrenean orogeny and

Austrian compressional phases before the formation of the ocean. In the second theory, the origin of magmatism in Iran involves the subduction of the Neo-Tethys oceanic crust beneath Central Iran. According to tertiary magmatism researchers, subduction models are more reliable than continental rifting in describing magmatism (7, 8) studying the evolution of the orogenic belt in the area between Kerman and Niriz states that the northern Neotethys subduction zone is the cause of the formation of the Sanandaj-Sirjan magmatic arc in the Mesozoic, and the southern subduction zone is the cause of the formation of the Niriz magmatic arc, a volcanic belt. Central Iran has porphyry copper deposits and the extensional environment behind the Rafsanjan Arch. He stated that the collision of the Arabian crust with Central Iran happened during the Neogene. In their studies (9), consider the Eocene magmatism to be post-collision, which breaks the oceanic plate after the collision and causes melting of part of the asthenosphere

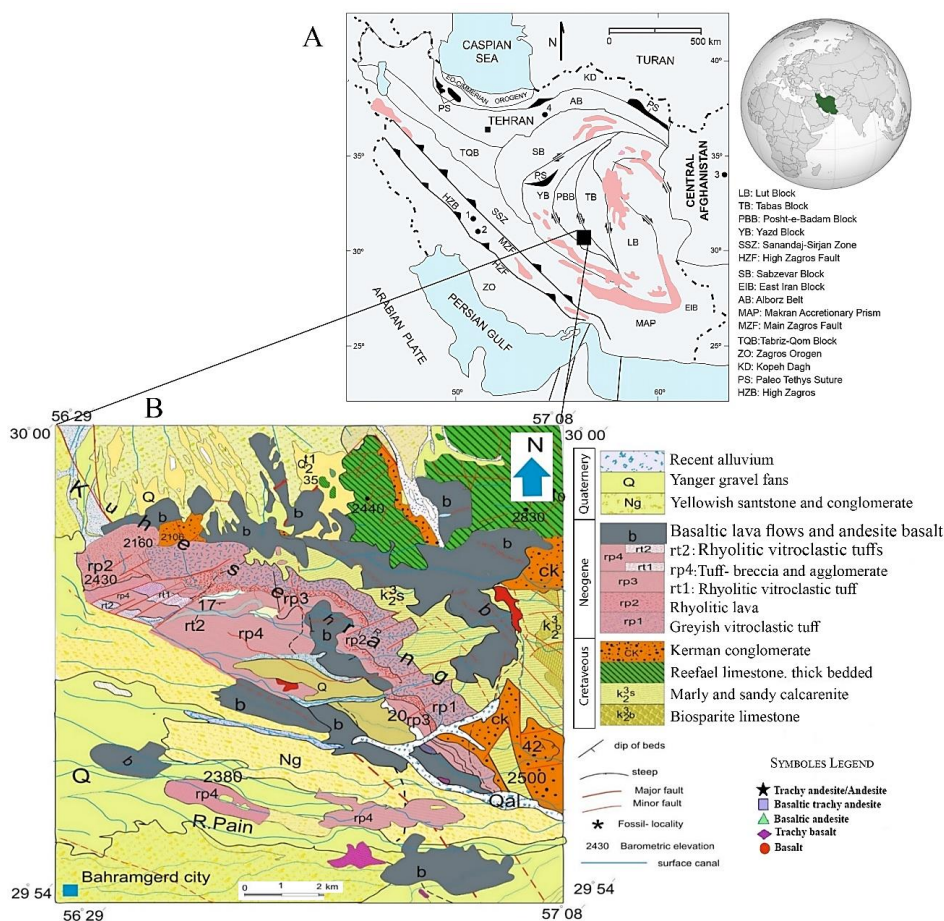


Figure 1. A) Generalized tectonic zonation of Iran (1), B) Geological map of Goloumak area (12) with correction, the symbols used in the figures in the text are given in the legend section.

under the crust of central Iran, and subsequently magmatism occurs (10). Considered the rocks of Harjand gabbro (Kerman province) in an intra-plate tectonic environment, in their opinion, the development of mafic rocks (mainly gabbro) of Harjand can be related to the extensional phase and the rise of melt from the asthenosphere mantle. Be in the continental rift (11) using geochemical and isotopic data of igneous rocks of Ijo deposits (in Shahr Babak) after the subduction of the Neotethys oceanic crust under the central Iranian plate, considered that the continental collision between the Arabian and Eurasian plates during the Mio- The Pliocene has led to the thickening of the crust, the failure of the subducting plate, and the

development of the asthenospheric window, and finally the partial melting of the subcontinental lithospheric crust, which has caused the development of copper-containing adakites in the Ijo region.

The study area is situated close to Goloumak Village, which is located around 30 kilometers south of Kerman (Figure 1). According to geological data, the volcanic rocks in the Goloumak area are from the Neogene period (12). Petrography and mineral chemistry, whole rock geochemistry, and the Sr-Nd isotope composition of volcanic rocks are all part of our research. Study the petrogenesis of post-collisional magmatism and show how the geochemical trends in each magmatic episode can influence the geodynamic



Figure 2. A) Basaltic rock units placed on older rhyolitic rocks. B- Andesite unites in north northwest of the study area. C- Placement of orange to red trachy basalts on green olivine basalts. D- thickness about 20-30 meters from the basaltic andesite flow. E- The effect of erosion in basalts and form spheroid showing core-stone and outer weathered shell. F- andesitic dyke in rhyolite units.

processes.

Geological setting

The Goloumak area in Central Iran, specifically the southern region of the Poosht Badam zone, hosts upper Cretaceous deposits and Neogene volcanic rocks. The volcanic rocks are felsic (rhyolite and dacite) and intermediate rocks (andesite basalt, andesite, and trachy-andesite), as well as mafic rocks like basalt and trachy-basalt, which are of Neogene age. In various regions, lava flows composed of basaltic and andesitic units can be observed overlying acidic rocks. In certain regions, the high temperature of the basaltic lava has caused the underlying deposits to undergo thermal alteration, resulting in a change in the color of the rocks to a reddish hue (Figure 2-A to C). Based on stratigraphic research, it has been determined that the acidic units are some of the oldest igneous units that have undergone considerable alteration. It is expected to find lava flows that consist of mafic and acidic rocks, which are dark gray to black and have a thickness ranging from 5 to 50 meters. Exfoliation weathering is considered a surface phenomenon, and on occasion, contraction fissures may form dark basaltic round balls (Figure 2-D-E). The andesitic rocks in the study are visible in both lava and dyke forms. In this area, there are many dykes composed of basaltic andesite and andesite (Figure 2-F). Most of the dykes are 2-3 meters wide and trend in the northwest-southeast direction.

Materials and Methods

During the field study, we collected approximately 250 samples and studied 25 thin sections of volcanic rocks from the Goloumak area using a polarizing microscope. The major and trace element compositions of 25 samples with the minor alteration were determined using ICP-MS by Lab West Mineral Analysis LTD in Australia, using inductively coupled plasma-atomic emission spectrometry (ICP-MS). Sr and Nd isotope ratios were determined for four samples using a rock/mineral/ash digestion process in a concentrated HF: HNO₃ solution. The digestion process was done out in closed Teflon beakers at 140°C for 48 hours. The resulting solution was dried and converted into nitrate. Geological silicate samples were analyzed for Sr and Nd isotopes using a modified chromatographic separation scheme. The scheme described in the literature is comparable to this one (13). Sr was analyzed as a 0.2% HNO₃ solution with 200ppb concentration, using NIST's SRM987 as the reference standard. The normalizing value for ⁸⁷Sr/⁸⁶Sr was 0.710255. Nd isotopes were analyzed as 50 ppb 2% HNO₃ solutions

using a Nu Instruments desolating nebulizer with plate number 1. JNdi was the reference standard for ¹⁴³Nd/¹⁴⁴Nd, with a normalizing value of 0.512115. (14) JNdi-1: a neodymium isotopic reference that is consistent with LaJolla neodymium.

Results and Discussion

Petrography

The rocks in the study area can be classified into acidic, intermediate, and basaltic groups. Andesites and trachy-andesites are more abundant than basalts. The intermediate rocks of the studied area are divided into three groups: pyroxene andesite, andesite and trachyte-andesites

Pyroxene-andesite rocks in the sample display various bright, brown, and dark green colors. The dominant texture of these rocks is porphyry, with plagioclase and pyroxene microlitic minerals forming the matrix. Pyroxene is in lower amounts, typically around 20-30% of rock volume. These minerals have euhedral to subhedral shapes, while the amount of ferromagnesian silicate minerals such as amphibole and biotite in these rocks is minimal (Figure 3-A). Hornblende and biotite include 5- to 10% volumes of Two-pyroxene-andesite. Plagioclase crystals exhibit polysynthetic twinning and are subhedral to euhedral. Plagioclase phenocrysts contain a core with a sieve texture, occupying approximately 55% of the rock's volume.

Andesite rocks are primarily composed of porphyry with a dominant texture. The matrix consists of plagioclase microlitic pyroxene, filled with opaque minerals and glass. In comparison to the pyroxene group of andesite-bearing rocks, this category of rocks lacks pyroxene (Figure 3-B). Their texture is porphyritic-hyaline, porphyritic-phaneritic with matrix microlitic and flow. The rocks contain primarily plagioclase and hornblende minerals, which include euhedral, subhedral phenocrysts and, microlites, often exhibiting zoning and sieve texture. Plagioclase crystals can reach up to 3 mm in size, but sometimes they are degraded at the margins. This could be due to differences in hydrothermal water accessing different parts of the crystal or variations in chemical composition between the crystal's center and margin. The rocks known as amphiboles often feature minerals whose opacity has increased. Some samples show hornblende with opaque and alternating margins (Figure 3-B). Some hornblende exhibits a poikilitic texture, where one large crystal encloses many smaller crystals. In addition, there are inclusions in minerals of the apatite. Accessory minerals present in these rocks

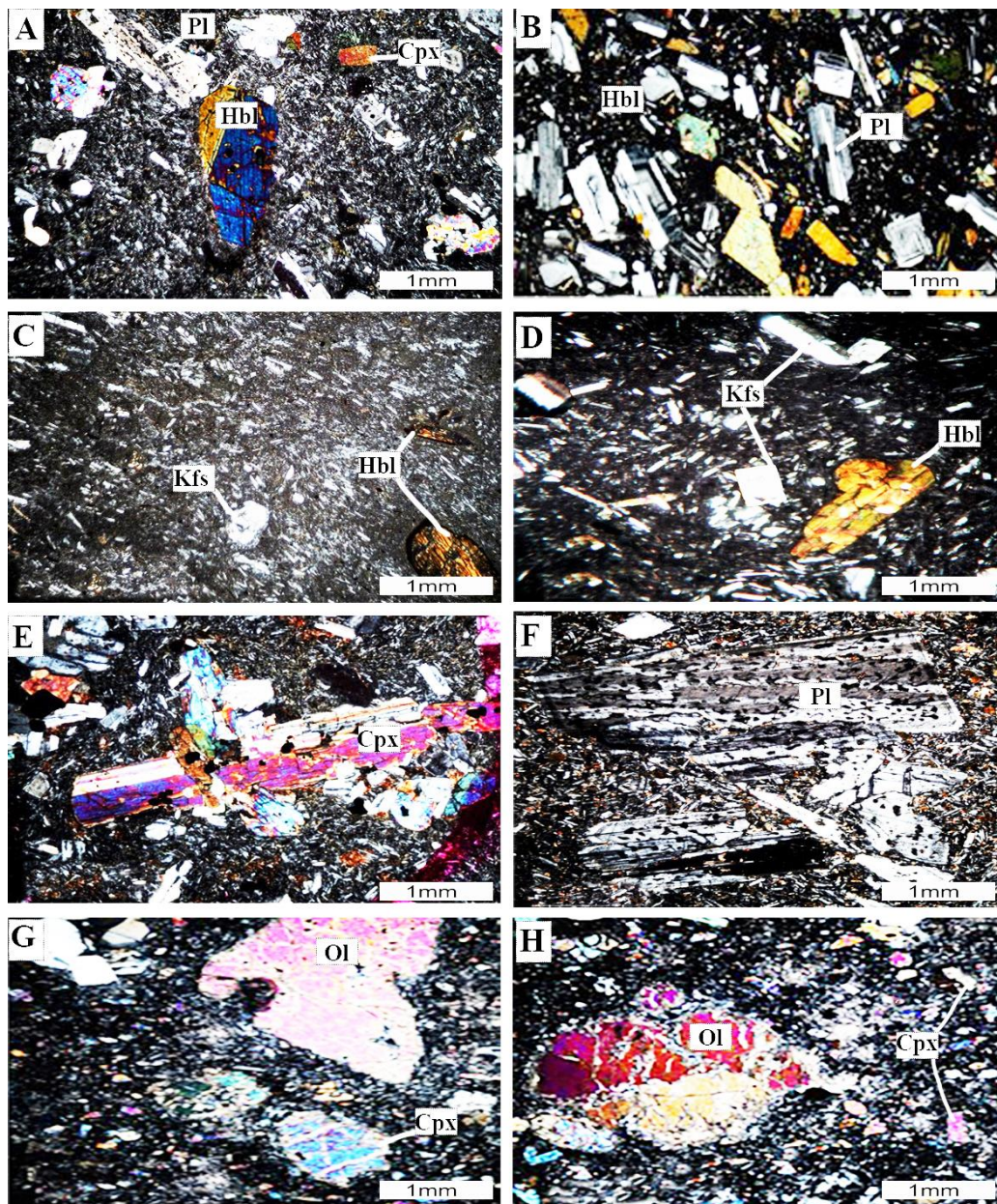


Figure 3. A) Pyroxene, plagioclase, and amphiboles are the main ingredients in the porphyritic texture made in pyroxene-andesite. B) Porphyritic texture with phenocrysts of plagioclase and hornblende in andesite rocks. C) Flow texture with alkali feldspars and hornblende phenocrysts in trachy-andesite. D) Flow texture with alkali feldspars with Carlsbad twinning and hornblende phenocrysts in trachy-andesite. E) Porphyritic texture with clinopyroxene phenocrysts and olivine in Basalt. F) porphyritic texture in basalt with zoned plagioclase phenocrysts. G) porphyritic texture in olivine-basalt rocks with olivine and clinopyroxene phenocrysts; some olivine minerals show reactive margins. H) porphyritic texture in olivine-basalt rocks with olivine and clinopyroxene phenocrysts. (Hbl =Hornblende, Pl = plagioclase, Cpx = Clinopyroxene, Kfs = Alkali feldspar and Ol= Olivine.) (16)

include apatite, sphene, alkali feldspar, augite, and opaque minerals. The presence of xenolith of basaltic quartz in these rocks is less common and predominantly occurs in the matrix, mixed with feldspar, which is hardly distinguishable.

The trachy-andesitic rocks are fine-grained and display a red to pink color. They have a porphyritic texture, wherein microcrystalline groundmass is present. These rocks have a higher concentration of K-feldspar than plagioclase and biotite. Sanidine, which is a type of

K-feldspar, is a common mineral and is slightly altered into clay minerals. Regarding phenocrysts, sanidine crystals are the most abundant, comprising 30-35% of the rock volume. Euhedral to subhedral K-feldspar is presented by tabular and prismatic phenocrysts, as well as small laths in the groundmass (Figure 3C-D). Amphibole phenocrysts range in size from 0.3 to 1.0 mm and vary in abundance from 2 to 10 vol%. These phenocrysts exhibit the typical form of amphibole and are often subhedral but can be altered to opaque minerals. (Figure 3-D). Biotite, partially altered to chlorite, forms prismatic crystals that are subhedral in shape. These crystals can measure up to 2.5 by 1.5 mm in size.

Basalt rocks found in the Goloumak area are porphyritic and hypocrystalline. The primary mineral assemblage comprises olivine, Ti-augite, plagioclase, and glass with different petrographic varieties. These rocks are gray, finely grained, and, vesicular. They contain phenocrysts of olivine, pyroxene, and plagioclase in an intergranular groundmass of plagioclase laths and other minerals. These rocks are composed of plagioclase (about 60%), olivine (about 30%), pyroxene (about 10%), and opaque minerals, mainly magnetite (as shown in Figure 3-A-B). The primary minerals appear as subhedral to euhedral phenocrysts, and microphenocrysts. Plagioclase minerals are often euhedral, displaying a sieve texture and Carlsbad twinning. In olivine basalts, plagioclase minerals are typically zoned. There is a change in the shape and size of the phenocrysts, Olivine phenocrysts and microphenocrysts range from colorless to pale grey and vary in size from 0.8 mm to 2 mm, displaying seriate texture. The larger olivine grains show moderate fracturing and alteration to iddingsite and chlorite along the crystal edges and fractures. The severity of iddingsite alteration may be related to the iron content of the crystals (15). The sample contains clinopyroxene crystals that range in color from colorless to light brownish, with twinned and sector-zoned phenocrysts. These crystals have a sieve texture and can grow up to 2.0 mm in length. The color of the clinopyroxenes can vary from colorless and pale brown to a faint purple, due to the presence of titanium. The habit of these crystals ranges from prismatic and granular to anhedral poikilitic grains. Olivine and plagioclase grains can be found enclosed by pyroxene plates. The pyroxenes often display zoning, increasing the intensity of the purple color towards the crystal margins.

The basaltic andesite outcrop exhibits various textural features such as porphyritic, vesicular, and intersertal textures within pyroxene, and large subophitic textures of plagioclase enclosed by pyroxene

crystals (Figure 3-E). The basaltic-andesite samples are mainly composed of clinopyroxene (Diopside), calcic-plagioclase, olivine, and magnetite, as well as secondary minerals such as iddingsite, zeolite, calcite, and quartz. The rock contains a high percentage of clinopyroxene, close to 50-60% of the rock's volume (Figure 3-E-F). The basaltic-andesite samples are mainly composed of clinopyroxene (Diopside), calcic-plagioclase, olivine, and magnetite, as well as secondary minerals such as iddingsite, zeolite, calcite, and quartz. The rock contains a high percentage of clinopyroxene, close to 50-60% of the rock's volume.

Geochemistry

The analysis of the chemical composition of geological samples has been presented in Table 1. The rocks studied in the TAS diagram (17) range from basaltic andesite to trachy-basalt, basalt, andesite, trachy-andesite, and basaltic trachy-andesite. The majority of the rocks are trachy-andesite (Figure 4). Diagrams (18, 19) (Figure 5) show that mafic rocks are alkaline and transition series and, intermediate rocks are calc-alkaline and transition series.

The pattern of rare earth elemental normalized to chondrite (20) shows a gradual decrease in the concentration of rare earth elements (LREE) to heavy (HREE) with negative slopes. This point can be shown with $(La/Sm)_N$ ratios of 2.51-6.82, $(Sm/Yb)_N$ 2-4, $(La/Yb)_N$ 5.9-17.28. The depletion of HREE elements can be due to the segregation of olivine, zircon or, hornblende minerals (21, 22). The enrichment of lightweight rare earth elements is related to two low-melting degrees. These include enriched mantle sources (<15%) and magma contamination by crust material. The La/Sm ratio is representative of LREE/HREE ratios and can express the role of each of these factors. If there is crust contamination due to the richness of the crust from LREES, the amount of La/Sm ratio should be high in the studied rock. Based on the comparison of the mean ratio $(La/Sm)_N$ in crust rocks (4.25) with the ratio of the studied rocks (3.99), it is likely that the studied rock has been contaminated with crustal materials. It is worth noting that this ratio tends to be higher in basaltic rocks (5.03), which further supports the idea of crustal contamination. However, based on the nature of alkaline mafic samples, the magma of these rocks can be derived from a lower melting degree of a source of enriched mantle. Most studied rocks show negative Eu anomaly ($Eu/Eu^*=0.71-1.01$) (average 0.78). The value of the Eu/Eu^* ratio for Jopar rocks decreases from mafic to acidic pole (for acidic rocks with an average of 0.66 and mafic rocks with an average of 0.825) (Figure 6).

In summary, mafic and intermediate rocks have

Table 1. Whole rock major oxides (wt. %), and trace elements (ppm) of chemical analyses of Goloumak area samples

Sample	J-20	J-27	J-35	J-43	J-53	J-75	J-90	J-116	J-127	J-138	J-140	J-143	J-151
SiO ₂	52.07	59.62	53.44	59.23	55.23	56.9	60.01	54.44	52.56	55.64	54.99	55.04	58.14
Al ₂ O ₃	16.42	16.91	17.06	16.12	17.43	17	16.96	16	17.03	17.38	16.58	17.18	16.48
Fe ₂ O ₃ t	9.51	6.21	9.43	6.26	6.66	5.99	6.02	9.01	10	7.1	8.9	7.35	7.1
CaO	9.57	4.96	7.56	5.01	8.02	5.56	4.98	7.52	7.89	7.99	7.34	8.6	6.12
K ₂ O	2.07	3.69	3.04	3.29	5.73	3.89	3.8	3.62	3.02	2.12	1.94	2.02	2.69
MgO	5.41	1.9	3.11	3.29	0.47	2.89	1.23	2.02	3.11	2.02	2.85	2.12	2.66
MnO	0.15	0.13	0.18	0.13	0.11	0.14	0.19	0.18	0.15	0.14	0.17	0.14	0.11
Na ₂ O	2.66	4.27	4.23	4.44	3.16	3.78	4.28	4.25	4.23	3.23	3.63	3.33	3.56
P ₂ O ₅	0.25	0.23	0.4	0.22	0.31	0.26	0.34	0.31	0.41	0.32	0.33	0.34	0.33
SO ₃	<0.05	0.1	0.1	0.05	<0.05	0.3	0.15	0.6	0.12	0.07	0.1	0.07	0.07
TiO ₂	0.97	0.72	1.15	0.94	0.89	1.08	0.85	0.96	1.12	0.89	0.96	0.89	0.84
Cr ₂ O ₃	<0.01	<0.01	<0.01	0.01	<0.01	<0.01	<0.01	<0.01	<0.01	<0.01	<0.01	<0.01	<0.01
LOI	0.82	0.97	0.97	0.87	1.82	2.02	0.99	1	1.12	2.96	2.85	2.96	2.23
Total	99.9	99.71	100.67	99.86	99.83	99.81	99.8	99.91	100.76	99.86	100.64	100.04	100.33
Ag	0.06	0.07	0.07	0.1	0.2	0.06	0.09	0.06	0.06	0.11	0.13	0.11	0.22
As	<0.5	3.4	1.7	4.8	4.3	14	2.5	12.9	1.7	3.8	4	3.3	7.7
Ba	491	622	567	722	605	692	737	737	601	692	662	626	625
Be	1.8	1.9	1.9	2.3	1.8	20	2.4	1.9	1.7	3.4	1.75	2.1	1.8
Bi	<0.1	0.1	<0.1	<0.1	<0.1	<0.1	<0.1	<0.1	<0.1	<0.1	<0.1	<0.1	<0.1
Cd	0.11	0.09	0.1	0.1	0.39	0.1	0.14	0.1	0.1	0.18	0.19	0.13	0.06
Ce	37.6	51.1	52.5	58.4	53.9	58	66.8	51	54.4	50	59.3	52.5	57.5
Co	29.4	14.9	13.6	9.5	18	12.8	7	15.3	12.89	11	14	12	11.6
Cr	32	53	<2	3	19	8	4	7	<2	19	18	15	7
Cs	1.1	2.9	1.1	4.8	2.82	3	2	4	1.8	3.7	9.1	3.1	8.4
Cu	37.7	31.2	12.2	19	39	28	20.5	19.8	11.45	39	33.8	34.2	24.4
Dy	4.26	3.88	5.64	4.93	4.96	3.8	4.95	4.68	4.62	3.6	4.76	4.67	5.14
Er	2.53	2.42	2.37	2.97	2.52	2.39	2.99	2.75	3.01	2.93	2.97	2.79	2.6
Eu	1.29	1.12	1.63	1.33	1.23	1.5	1.41	1.53	2.1	1.74	1.74	1.35	1.39
Ga	20.1	16	18.3	17.2	18.2	18	17.2	17.8	19.1	19.9	16.1	17.6	18.1
Gd	4.7	4.33	6.19	5.64	5.74	5.7	5.56	5.33	6.91	5.81	6.01	5.18	6.33
Ge	0.93	0.82	0.85	0.85	0.19	0.1	0.86	0.8	0.58	0.71	0.99	0.75	1.12
Hf	2.69	4.35	4.04	4.43	3.39	4.93	4.54	4.49	4.7	3.39	3.39	3.93	3.05
Hg	<0.05	<0.05	<0.05	<0.05	0.05	<0.05	<0.05	<0.05	<0.05	<0.05	<0.05	<0.05	<0.05
Ho	0.87	0.8	1.16	1.01	1.03	0.91	1.02	0.95	1.06	1.01	0.95	0.95	1.08
In	0.06	0.04	0.06	0.05	0.05	0.06	0.05	0.04	0.06	0.05	0.05	0.05	0.05
La	19.6	28.2	26.6	30.8	28.7	29	35.6	27.1	25.7	30.8	29.8	28.1	28.8
Li	10.2	15	12.4	8.2	7.6	4.8	17	8.4	12.2	7.5	8.6	9.1	15.2
Lu	0.32	0.33	0.44	0.39	0.47	0.3	0.4	0.35	0.31	0.41	0.38	0.37	0.33
Mo	1.4	2.3	1.7	1.8	1.2	1.2	2.3	1.5	1.6	1.9	1.5	1.7	2.1
Nb	6.3	6.9	7	7.7	6.7	7	9.4	7	6	6.71	8.1	6.8	5.4
Nd	18.9	21.6	26.7	26.9	21.9	29.3	28.4	23.9	26.3	22.6	22.3	24.1	27.5
Ni	8	15	<2	<2	5	3	<2	2	<2	8	5	4	<2
Pb	13.8	19.5	12.4	18.4	29.1	17.1	35.6	16.9	12	29	23.4	22.6	12
Pr	4.52	5.68	6.34	6.73	6.1	5.78	7.52	5.94	6.43	6.85	6.78	6.05	6.74
Rb	88.3	136	75.8	103	174	119	120	116	57.9	193	142	137	228
Re	<	<	<	<	<	<	<	<	<	<	<	<	<
	0.0005	0.0005	0.0005	0.0005	0.0005	0.0005	0.0005	0.0005	0.0005	0.0005	0.0005	0.0005	0.0005
Sb	0.4	0.3	0.1	0.3	0.2	0.9	0.3	0.3	0.1	0.9	0.3	0.3	0.5
Sc	27	14	19	12	14	17	10	17	21	15	13	17	19
Se	0.48	0.3	0.31	0.29	0.63	0.48	0.36	0.33	0.48	0.26	0.74	0.62	0.38
Sm	4.59	4.57	6.27	5.97	5.34	5.7	5.97	5.5	6.6	5.14	5.96	5.34	6.44
Sn	1.2	1.6	1.4	1.5	1.7	1.1	1.7	1.3	1.9	1.9	1.7	1.4	1.1
Sr	633	506	577	599	693	690	504	629	573	628	651	656	446
Ta	0.34	0.54	0.5	0.61	0.5	0.29	0.72	0.52	0.5	0.5	0.4	0.5	0.38
Tb	0.74	0.68	0.98	0.86	0.76	0.773	0.85	0.83	0.99	0.71	0.83	0.81	1
Te	<0.2	<0.2	<0.2	<0.2	<0.2	<0.2	<0.2	<0.2	<0.2	<0.2	<0.2	<0.2	<0.2
Th	4.54	8.78	5.6	8.28	7.12	9.3	8.57	6.72	6.1	9.01	6.14	6.9	4.83
Tl	0.2	1.6	0.3	1.9	2.9	1.5	0.6	2.8	0.3	2.7	3.42	2.2	0.9
Tm	0.35	0.35	0.4	0.42	0.38	0.39	0.42	0.38	0.4	0.32	0.38	0.4	0.42
U	1.46	2.61	1.8	2.59	3.12	1.9	2.62	2.03	1.9	2.21	2.74	2.33	3.37
V	242	130	223	128	192	172	88	186	232	182	17.9	184	224
W	0.7	1.2	0.9	1.1	1	0.8	1.3	0.9	0.8	1.7	2.4	1	13.3
Y	30.8	23.8	33	29.1	24.9	20.9	29.6	27.2	31	28.2	25.8	27.8	34.5
Yb	2.28	2.32	3.07	2.71	2.7	2.83	2.86	2.49	3.12	2.4	2.83	2.6	2.45
Zn	104	72.2	88.3	80.4	94.5	80.4	95.6	83.3	82.9	93.7	96.7	94.8	111
Zr	180	171	177	201	193	191	171	184	169	210	186	203	188

partially negative anomalies, while acidic samples exhibit more negative anomalies. The negative anomaly indicates the separation of feldspar from the melt during crystal fractionation or partial melting or high oxygen fugacity during fractional crystallization of magma (23).

Since the mentioned anomaly in the studied rocks (especially basalts) is tiny, it indicates that the partial crystallization and subtraction of plagioclase played a small role in the evolution of the magma that produced these rocks.

Table 1. Continued

Sample	J-164	J-167	J-174	B-12	B-13	B-30	B-41	B-52	B-53	B-64	B-71	B-78
SiO ₂	59.1	55.84	55.89	48.8	49.16	49.79	48.2	49.01	40.85	46.98	49.1	51.07
Al ₂ O ₃	16.02	17.2	17.41	16.6	16.92	16.95	17.4	17.21	11.32	13.9	14.6	16.95
Fe ₂ O ₃ t	6.29	6.82	7.6	9.95	10.01	9.23	10.5	10.54	10.65	8.63	11	9.25
CaO	6.59	7.97	7.55	9.75	7.49	9.82	10.01	9.83	14.01	13.28	8.5	8.77
K ₂ O	3.08	2.15	2.2	2.8	2.99	2.85	2.49	2.05	1.79	2.41	2.34	2.07
MgO	3.37	2.26	1.93	7.37	5.73	5.4	7.9	8.01	12.85	7.01	7.66	6.93
MnO	0.13	0.15	0.16	0.91	0.23	0.8	0.15	0.14	0.9	0.42	0.38	0.15
Na ₂ O	3.55	3.32	3.62	2.01	3.24	2.8	2.01	2.11	2.51	2.9	3.5	2.53
P ₂ O ₅	0.22	0.34	0.3	0.74	0.89	0.72	0.75	0.42	0.79	0.48	0.34	0.45
SO ₃	0.05	0.07	0.07	0.05	0.05	0.06	<0.05	<0.05	<0.05	0.06	0.06	<0.05
TiO ₂	0.67	0.81	0.82	0.96	1.52	0.82	0.97	0.59	2.42	2.59	1.5	0.98
Cr ₂ O ₃	<0.01	<0.01	<0.01	0.01	0.01	<0.01	<0.01	<0.01	0.09	<0.01	<0.01	<0.01
LOI	1.89	2.53	2.97	2.1	1.8	1.93	0.82	1.11	1.14	2.56	2.09	1.03
Total	100.96	99.46	100.52	102.05	100.04	101.17	101.2	101.02	99.32	101.22	101.07	100.18
Ag	0.22	0.36	0.15	0.14	0.16	0.19	0.2	0.17	0.19	0.25	0.18	0.44
As	8.01	3.17	3.7	3.8	2.8	3.3	4.3	3.6	2.12	3.7	3.6	3.18
Ba	712	628	686	499	491	459	410	450	389	428	450	498
Be	1.9	3.2	3.3	2.8	1.8	2.6	2.3	2.7	1.2	1.96	2.5	2.5
Bi	< 0.1	< 0.1	< 0.1	0.1	< 0.1	0.1	0.1	0.1	0.11	0.1	0.1	< 0.1
Cd	0.04	0.82	0.19	0.18	0.2	0.11	0.3	0.6	0.9	0.8	0.8	0.92
Ce	59.9	59	56	93	80	82	80	96	102	95	90	81
Co	10.2	15	18	25.2	29.4	25.8	21.2	20.7	23.45	25	25.7	30.4
Cr	8	21	22	185	190	155	103	141	170	152	154	123
Cs	8.9	3.89	3.45	135	111	143	120	158	170	130	142	162
Cu	23.3	38.1	37.7	35	37.7	37.7	39	32.81	39	36.3	37	38.4
Dy	5.01	4.11	4.01	4.2	4.26	5.12	Apr-80	4.6	4.75	5.23	5.5	4.89
Er	3.07	2.76	2.84	2.32	2.53	3.18	3.01	2.72	3.1	2.99	2.2	2.35
Eu	1.93	2.1	1.81	2.51	1.29	1.61	2.02	1.79	2.11	2.1	1.4	1.61
Ga	14	18.45	17.6	16.1	20.1	15.4	11.92	16.1	15.2	15.15	16.7	21.5
Gd	6.2	5.96	5.81	7.7	6.3	7.22	7.62	6.81	7.7	6.89	6.25	7.4
Ge	1.1	0.73	0.81	0.84	0.93	0.78	0.72	1.1	0.99	0.72	0.71	0.93
Hf	3.9	3.4	3.6	4.53	3.8	4.51	4.4	4.02	4.6	4.12	4.11	3.58
Hg	< 0.05	< 0.05	< 0.05	< 0.05	< 0.05	< 0.05	< 0.05	< 0.05	< 0.05	< 0.05	< 0.05	< 0.05
Ho	0.9	0.82	0.99	1.05	0.87	1.13	1.2	1.13	1.08	1.1	0.9	0.74
In	0.05	0.05	0.05	0.06	0.06	0.05	0.05	0.05	0.05	0.05	0.05	0.06
La	29	32.2	28.9	47	49	49	53	51	49	48	50	45
Li	18	7.5	7.6	45.45	30.5	45.6	40	42	45.2	46	45	39.1
Lu	0.47	0.4	0.36	0.31	0.32	0.4	0.31	0.3	0.4	0.4	0.26	0.36
Mo	2.9	1.8	1.9	3.75	1.4	2.1	3.1	3.3	2.93	2.41	2.7	2
Nb	5.7	6.71	6.42	29	23	28.5	25	27.1	28.5	27.45	28.3	24.6
Nd	29	22	22.6	38	35	33.2	40.2	39.6	45.1	37	36	36.3
Ni	< 2	9	8	68	60	64	62	60	68	62	65	68
Pb	19	28	24	17.5	13.8	20.6	19.2	22	21.6	20.2	21.1	15.5
Pr	6.7	6.48	6.52	8.9	7.52	8.6	8.3	10.1	9.38	9	7.69	9.01
Rb	283	211	194	110	88.3	97.4	92	96	98	95.9	97	89
Re	<	<	<	<	<	<	<	<	<	<	<	<
	0.0005	0.0005	0.0005	0.0005	0.0005	0.0005	0.0005	0.0005	0.0005	0.0005	0.0005	0.0005
Sb	0.7	0.9	0.6	0.8	0.4	0.4	0.5	0.4	0.4	0.5	0.3	0.6
Sc	26	16	17	19	27	17	19	19	14	18	19	21
Se	0.71	0.36	0.27	0.41	0.48	0.33	0.42	0.2	0.33	0.29	0.32	0.43
Sm	6.8	5.17	5.13	8.82	5	5.3	7.99	6.03	7.52	7.6	4.73	6.41
Sn	1.5	1.86	2.6	3.6	1.2	2.1	1.86	2.7	2.7	2.01	2.1	1.7
Sr	532	652	682	875	633	855	712	820	866	815	824	592
Ta	0.7	0.9	0.6	1.8	0.94	1.44	1.22	1.77	1.75	1.78	1.23	0.99
Tb	1.05	0.72	0.63	0.92	0.74	1.02	1.09	0.89	1.1	0.92	0.8	0.73
Te	0.2	< 0.2	< 0.2	< 0.2	< 0.2	< 0.2	< 0.2	< 0.2	< 0.2	< 0.2	< 0.2	< 0.2
Th	4.83	10.1	9.99	7	4.54	7.22	6.01	7.3	7.22	7.1	7.9	6.66
Tl	0.82	2.6	2.9	0.9	0.2	0.6	0.5	0.6	0.5	0.6	0.4	0.3
Tm	0.45	0.33	0.41	0.32	0.37	0.39	0.32	0.4	0.41	0.42	0.36	0.37
U	4.4	2.12	2.85	3.87	1.46	3	5	4	4	3	4	2.83
V	293	183	189	143	242	140	162	123	145	151	148	180
W	14.6	1.8	1.9	2.45	0.7	2.3	2.8	2.02	2.6	2.7	2.4	2.1
Y	39	28.4	27.9	39	30.8	33	35	39	31	39	35	29.4
Yb	2.71	2.04	2.6	2.92	2.28	2.82	2.2	2.73	2.58	2.85	2.1	2.04
Zn	192	96	94.45	87	104	88	90	82	81	102	80	115
Zr	193	182	194	186	179	193	205	203	192	175	184	188

Multi-element diagram normalized to the primary mantle and chondrite (20, 24) for volcanic rocks from the Goloumak area shows specific depletion in Ba, Ti, Nb, Ta and enrichment of K, Rb, Th (Figure 7-A).

Multi-element patterns normalized to the primitive mantle estimate of (20). This diagram illustrates the enrichment of Pb, Th, Rb, U, and K and the depletion in Nb, Ti, P, and Ba, (Figure 7-B). The studied rocks show

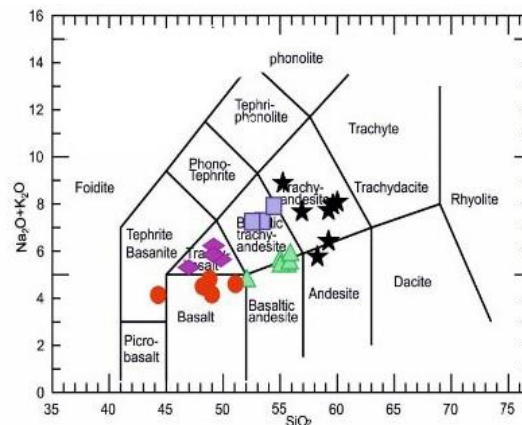


Figure 4. Plot sample of Goloumak area in Na₂O+K₂O versus SiO₂ (17).

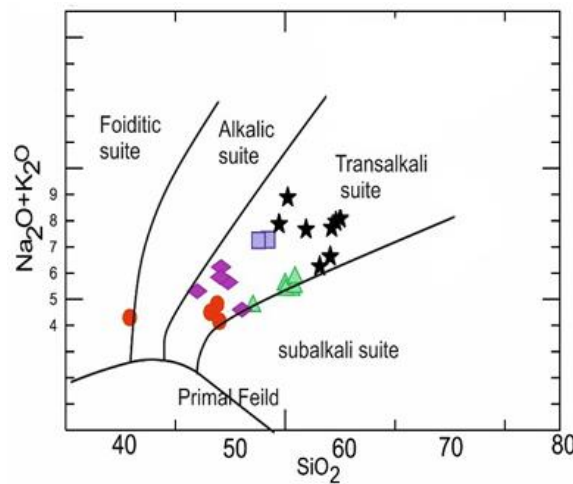


Figure 5. Shows the position of the Goloumak area's igneous samples in the magmatic series identification diagrams. SiO₂ Vs.Na₂O+K₂O diagram used for discriminating magmatic series of rocks (18-19).

signs of fractional crystallization of feldspar, apatite, and oxides, as evidenced by negative anomalies P, and Ti (25). The multi-element spider diagram (Ti, P, Ta, and Nb) indicates substantial contamination from continental crust in continental basalt. According to (26), depletion in Ta-Nb and enrichment of LIL, LREE can result from two factors: 1) the genesis of magma from an enriched mantle source (due to subduction fluids) and 2) crust contamination of mantle magma (27, 28). Although the observed anomalies, especially Nb-Ta, are the unique features of subduction regions spider diagrams, such anomalies have also been reported in basalt contamination by continental crust (flood basalts and continental rift) (27, 28). Positive anomalies of Pb and Cs can be affected by the contamination of continental crust during magma, because of the high concentration of these elements in the continental crust. Thus, stopping short-term magma and magma ascending of continental crust with crustal fluid into

magma can create these anomalies in studied rocks (27, 28).

Sr-Nd Isotope geochemistry

This research focuses on the mineralogy and petrogenesis of basaltic isotopic ratios to better understand the primary magma source and any contamination. Table 2 presents the results of four mafic rock samples, all with the same isotope composition. This suggests that they originated from a common source (29). ⁸⁷Sr/⁸⁶Sr Combination spectrum studied samples is 0.705935 to 0.706203, ¹⁴³Nd/¹⁴⁴Nd ratio is 0.51244 to 0.512509 with the value εNd -0.6 to -2.4. Figure 8 shows the Sr, Nd isotope correlation diagram; Goloumak area samples are located in a mantle array subjected to a relative enrichment of ⁸⁷Sr/⁸⁶Sr (Figure 8-A). Continental crust has an isotope ratio lower than Nd and a higher isotope ratio of Sr, while mantle magma has an inverse relationship (21, 30). According to the

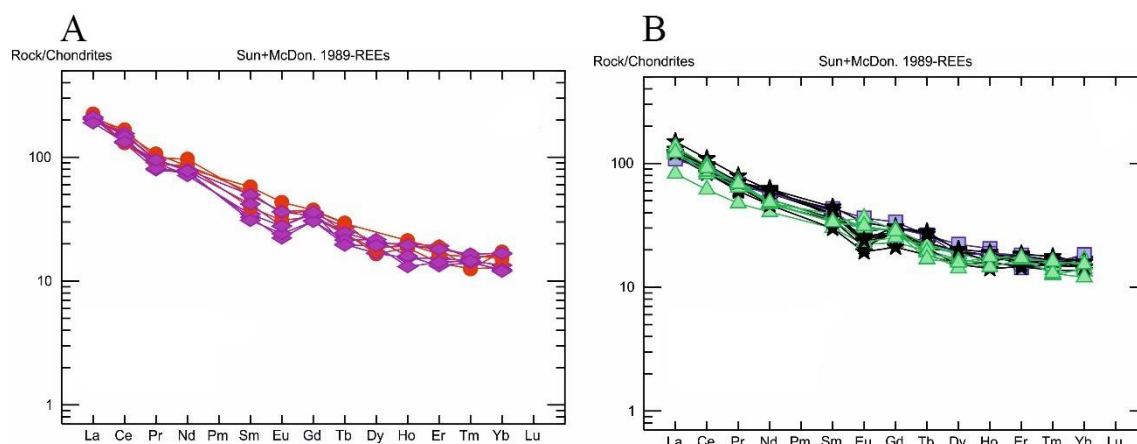


Figure 6. A) REE pattern in basaltic rocks of Goloumak area B- REE pattern in intermediate rocks of Goloumak area.

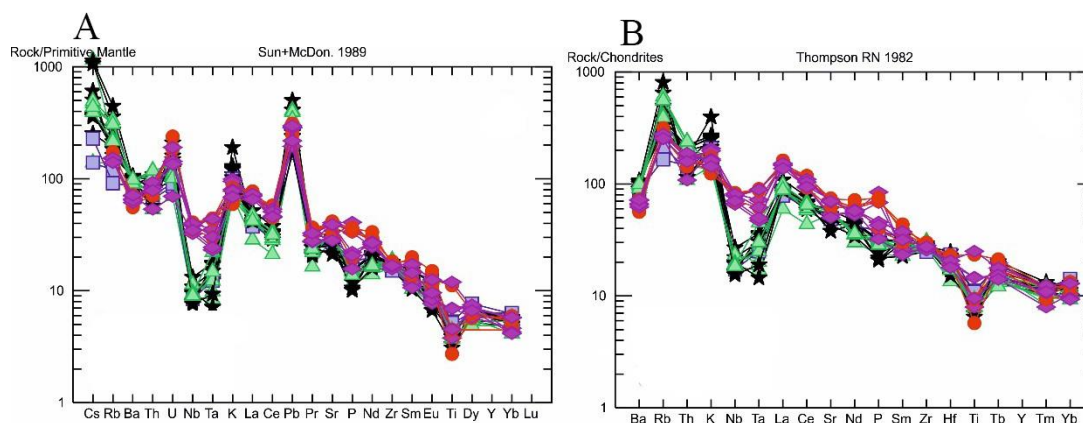


Figure 7. A)- Multi-element diagram normalized to the primary mantle (20) -B Multi-element diagram normalized to chondrite (24)

comparison of the studied samples in $^{143}\text{Nd}/^{144}\text{Nd}$ isotope correlation diagram versus $^{87}\text{Sr}/^{86}\text{Sr}$ (31), the mafic rocks of the Goloumak area are in the range of mantle affected by the subduction of lithospheric slab or metasomatic by mantle crust (Figure 8-B). In addition, the changes graph of $^{87}\text{Sr}/^{86}\text{Sr}$ against fluctuations of $^{143}\text{Nd}/^{144}\text{Nd}$ expresses that the mafic rocks have a mantle nature and, on the other hand, have been affected significantly by an amount s of crust material analyzed the mafic continental mantle array, the isotope ratio chart of $^{143}\text{Nd}/^{144}\text{Nd}$ against $^{87}\text{Sr}/^{86}\text{Sr}$ was used based on the isotope ratios of Nd in CHUR and Sr in UR. (32) A diagram is often divided into four sections to simplify the interpretation of data. Goloumak area basalts in the area of the fourth part (mantle array) with the low ratio of Sm/Nd ($F_{\text{Sm}<0}$), the depletion of Sm and the high ratio of (Rb/Sr $F_{\text{Rb}>0}$) rich from Rb probably are derived from rich resources of Rb and depletion of Sm and can be effective by contamination magma or is the

final product of geochemical differentiation of the mantle which indicates contamination of crust and initial magma. The rocks in this part are full of Rb with the depletion of Sm (32) (Figure 8-C). On the other hand, a draw of other chrons lines from Goloumak mafic rocks, $^{87}\text{Rb}/^{86}\text{Sr}$ versus $^{87}\text{Sr}/^{86}\text{Sr}$, shows these rocks have 12.5 Ma in age (Figure 8-D).

Tectonic setting and Petrogenetic evolution

The presence of two types of calc-alkaline magma and alkaline magma with different chemical compositions is a sign of volcanic activity in the Neogene block of the Goloumak area. It is necessary to look at the characteristics of primitive magmas that are in balance with the mineralogy of the upper mantle index (olivine + orthopyroxene + garnet + spinel). These features include high Mg# (>0.7), high Ni amounts (1400- 1500ppm), and High Cr (>1000ppm). However, for a standard mantle derived from regions of

Table 2. Initial Ratios for $^{87}\text{Sr}/^{86}\text{Sr}$ and $^{143}\text{Nd}/^{144}\text{Nd}$ of the Goloumak area basalts

Sample	$^{87}\text{Rb}/^{86}\text{Sr}$	$(^{87}\text{Sr}/^{86}\text{Sr})_i$	$^{87}\text{Sr}/^{86}\text{Sr}$	$^{147}\text{Sm}/^{144}\text{Nd}$	$(^{143}\text{Nd}/^{144}\text{Nd})_i$	$^{143}\text{Nd}/^{144}\text{Nd}$	ϵNd	TDM
B1	0.134036	0.705877	0.706203	0.146774	0.512345	0.512509	-1.4	1.457521
B2	0.656711	0.704606	0.706333	0.177195	0.512292	0.51249	-2.4	2.739786
B3	0.663101	0.704823	0.706435	0.124157	0.512301	0.51244	-2.26	1.207622
B4	0.380467	0.70501	0.705935	0.155849	0.512386	0.51256	-0.6	1.551535

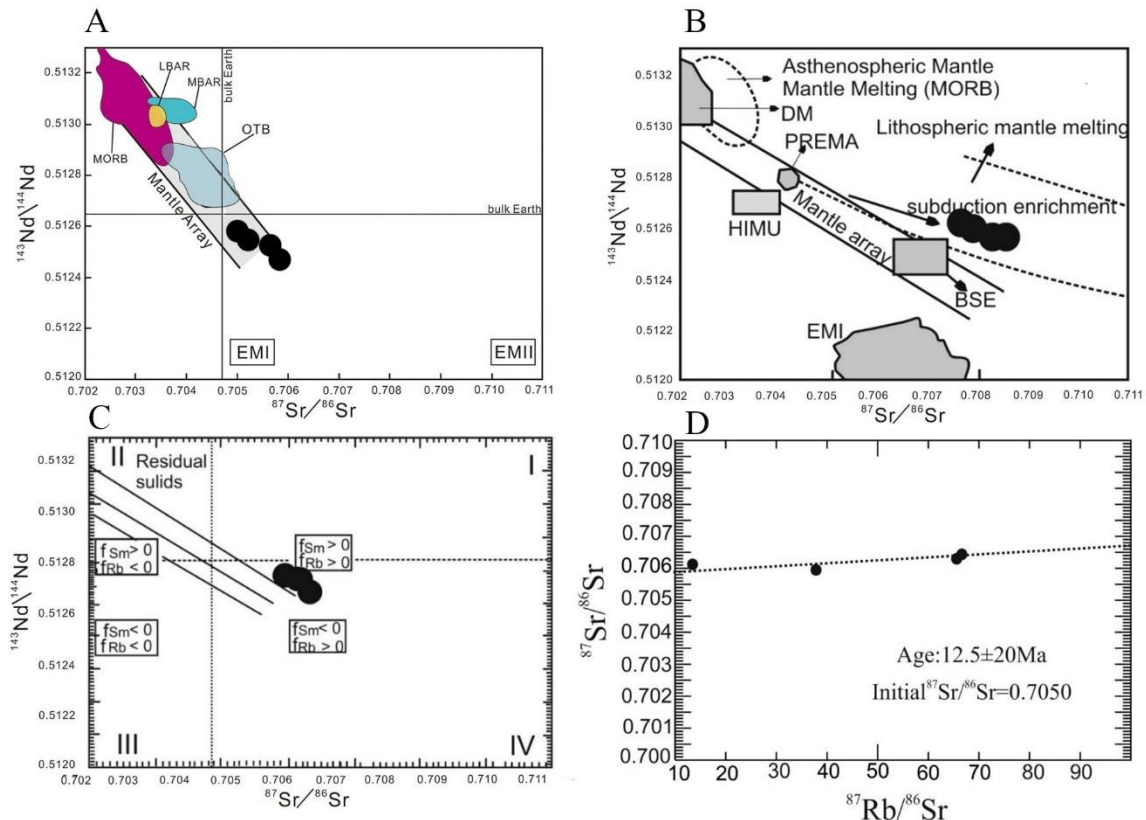


Figure 8. A) $^{143}\text{Nd}/^{144}\text{Nd}$ isotopic ratio versus $^{87}\text{Sr}/^{86}\text{Sr}$ in the studied area (33). B) Isotopic correlation diagram of $^{143}\text{Nd}/^{144}\text{Nd}$ against $^{87}\text{Sr}/^{86}\text{Sr}$ (31). C) Distribution of isotope ratios $^{143}\text{Nd}/^{144}\text{Nd}$ to $^{87}\text{Sr}/^{86}\text{Sr}$. D) Draw of isochrones line from Goloumak mafic rocks

metasomatic, these criteria will no longer be applicable (27). Goloumak area basalt has $\text{Mg}\# < 0.68$ and Ni, Cr amounts, respectively, less than 63, 153ppm. Thus, it can be concluded that the magma constituent of the studied rocks is not the primary magma part, and does not match the upper mantle. Therefore, after the formation in the initial mantle, it either undergoes changes or is the result of magma derived from a metasomatic mantle. The Magma of Goloumak area intermediate rock is calc-alkaline. There are different views on the origin of calc-alkaline magma. (34) believe in the primitive of such magmas, and scholars like (35), believe in the secondary genesis of such magmas. Andesite, especially orogenic andesite, can be seen in any four areas the plate tectonic setting. These areas are the boundary of divergent and convergent plates, intraplate, fault boundaries, and collision margin.

Mainly, orogenic andesite is in conjunction with the boundaries of convergent plates. Volumes of rocks with or without andesite can be in relative tectonic settings and the origin of andesite constructive magma. Orogenic andesite is generally associated with basaltic rocks. It is also influential in their formation in addition to tectonic setting, contamination, differentiation, or crust melting. Indeed, providing petrogenesis modeling for the production of intermediate magmas, in addition to considering geological facts of the area, must benefit from mineralogy and chemical results. According to mineralogical and geological evidence, calc-alkaline and alkaline magma of the Goloumak area are under the influence of AFC processes. To examine the effects of AFC processes, Ta/Yb-Th/Yb diagram was used (36). This diagram shows the interference of continental and lithospheric semi-continental in the placement of the

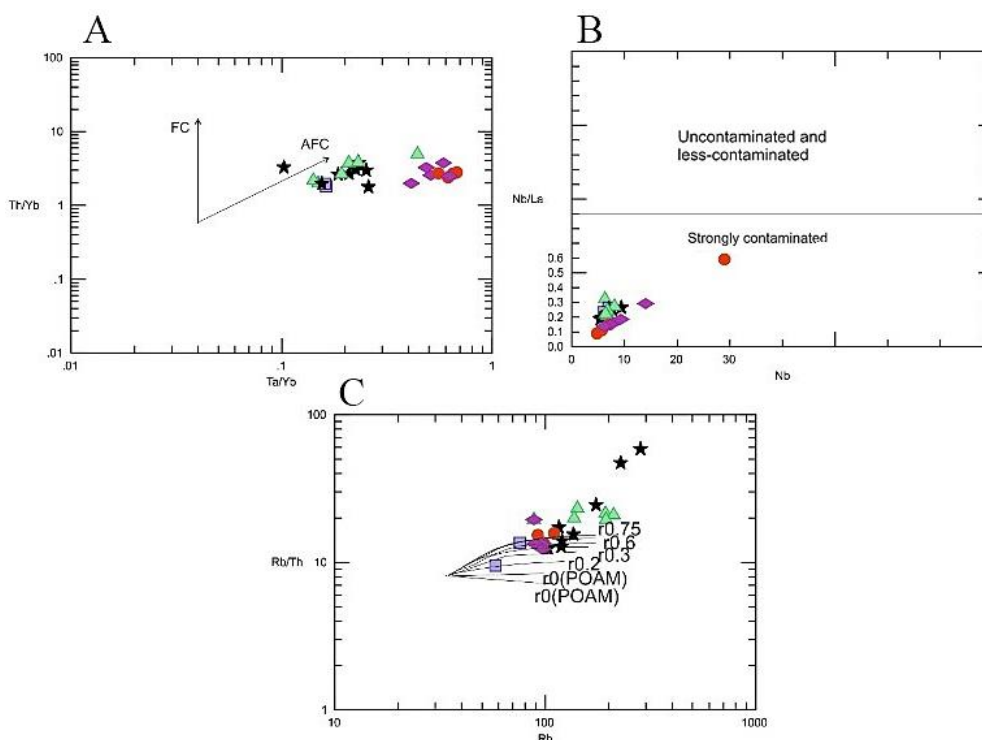


Figure 9. A)- Ta/Yb vs. Th/Yb diagram to review process AFC [(27). B) Nb vs. Nb/La diagram (38). C) Rb/Th vs. Rb diagram that represents the AFC process for studied rocks (38).

rocks and Ta/Yb-Th/Yb ratio changes for Goloumak area samples show the intervention of crustal contamination processes in pathogenesis formation of the magma producing these rocks (Figure 9-A). The climb of magmas produced in the mantle wedge from ticked crust can cause crust contamination and a low Nb/La ratio, which is the outcome of the low concentration of Nb in the studied rocks, and the result of crust contamination (Figure 9-B).

Model of Assimilation and Crystal Fractionation (AFC)

In this model, the Rb/Th ratio was used. The value of the Rb/Th ratio in crust rocks is greater than that of mafic rocks. Therefore, the increase in this proportion in the rocks of the study area could be due to crust contamination. In this diagram, Rb is a differentiation index. This model shows different degrees of fractional crystallization versus different amounts of (r) representing the ratio of assimilation rate to crystal fractionation; based on the figure, the more data from the analyses of rock become closer to the crustal composition, the more assimilation is done (37). Plotting the values for the rocks of the study area shows that the Goloumak area rocks are located close to the

crustal composition, so they have contamination and assimilation (Figure 9-C) (38). To determine the geodynamic setting from mafic and intermediate Goloumak area tectonic setting diagram developed was used in this diagram (Figure 10-A, B). The investigated samples plot in the Geotectonic diagrams (39) in Zr/Y versus Nb/Y and Nb/Th versus Zr/Nb diagrams shown island-arc setting. Volcanic arc basalts have a lower Ce/Sr ratio than MORB and intra-plate basalts, with the same amount of Cr. As seen in the diagram, the samples are within the range of volcanic arc basalts (Figure 10-C). In active continental arcs, there are different environments, such as back-arc collision environments and post-collision environments. The studied rocks are located in a past-collision arc.

The LREE/HREE ratio of the mafic and intermediate shows that the magma source originates from low partial melting to intermediate from the mantle. Generally, the enrichment of LREE can be attributed to two factors: Low Alkaline basalts show the low melting degree of the mantle in the formation of magma, and the calc-alkaline nature of intermediate rocks can indicate the impact of pollution processes in magma. Partial melting (<15%) of mantle source and magma contamination by crust materials. The alkaline

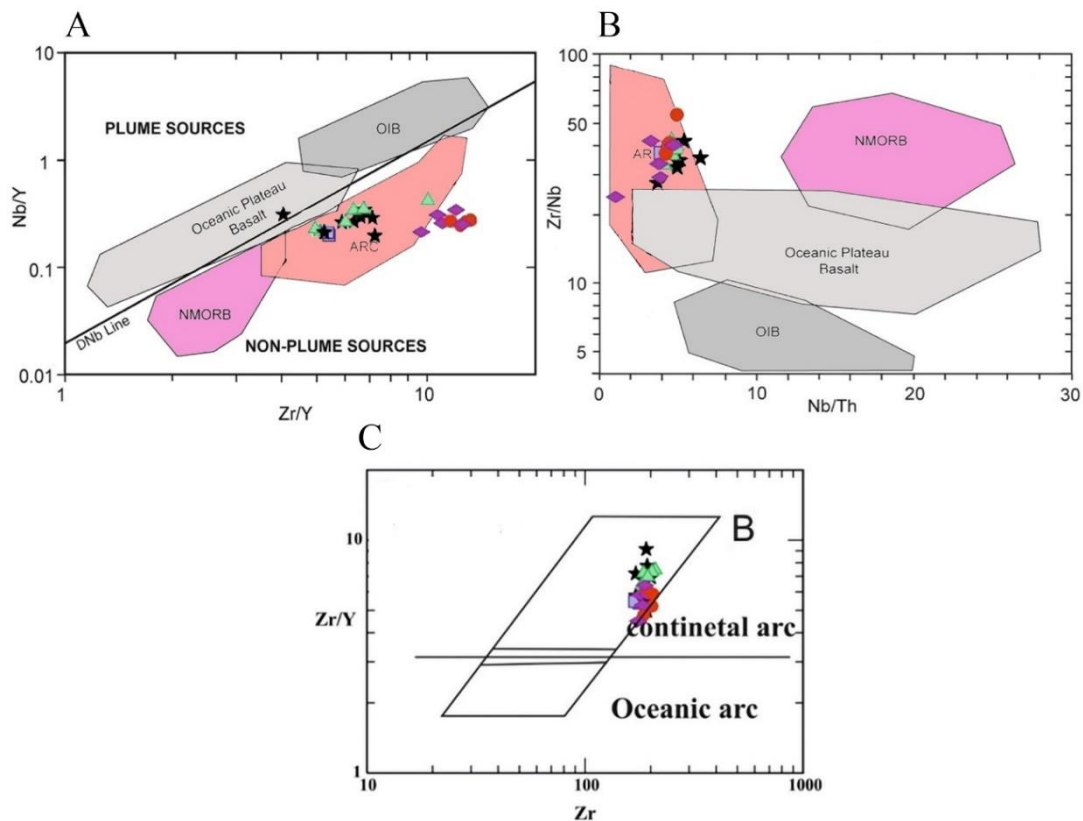


Figure 10. A) Zr/Y versus Nb/Y diagram[39], B) Nb/Th versus Zr/Nb diagram (39), C) Differentiation diagram based on Z vs. Zr/Y changes, oceanic and continental arc fields are separated based on $Zr/Y=3$ (27).

basalts express the low melting degree of the mantle in the formation of magma and, the calc-alkaline nature of the intermediate can express the contamination of magma. Depletion of these rocks of HREE in the source shows garnet in genesis. To calculate the amount of partial melting, La/Sm vs La was used (33). From the comparison of the composition of lava with the combination of magmas rooted in the melting of spinel or lherzolitic garnet, one can determine the degree of melting and the nature of the mantle of their origin. The studied abundance of La, Sm has a similar composition with magma derived from the enriched mantle on a process consistent with about 1% to 5% of the lherzolitic garnet (Figure 11-A). (40) believes that the transferring zone between spinel lherzolitic and garnet lherzolitic is at a depth of 60-80Km, and others believe that the transition zone between spinel lherzolite to garnet lherzolitic is at a depth of upper mantle (41, 42). Given that this graph shows the presence of garnet and the absence of spinel in the origin of rock in the region, it can be considered at least as the depth of the rooting of the magma, which forms these rocks from a depth of

more than 80 km. To prove the roots of the magmas of the studied rocks from the enriched mantle, the Zr/Y vs Zr diagram was used where all samples are in the range of enriched mantle (Figure 11-B). Diagram Nb/Zr vs Nb/Ba shows that the studied rocks have been created from the lithospheric mantle (43) (Figure 11-C).

Multiple mechanisms have been proposed to cause the melting of the mantle and the formation of alkali magmas. Decompression melting of the rising asthenosphere is a common occurrence in areas with thinned lithosphere. According to models, the volume of melt produced is influenced by the stretching factor of the lithosphere, as well as the temperature and composition of the asthenosphere (45). Mantle melting due to stretching in the solid lithosphere is closely related to the amount of stretching and the age of stretching in the studied area (33). For a peridotite mantle to melt in dry conditions, significant stretching must occur in the solid lithosphere (45). However, the meta-somatization of the mantle causes melting to start even in small amounts of elongation because the increase of volatile substances in the mantle causes the

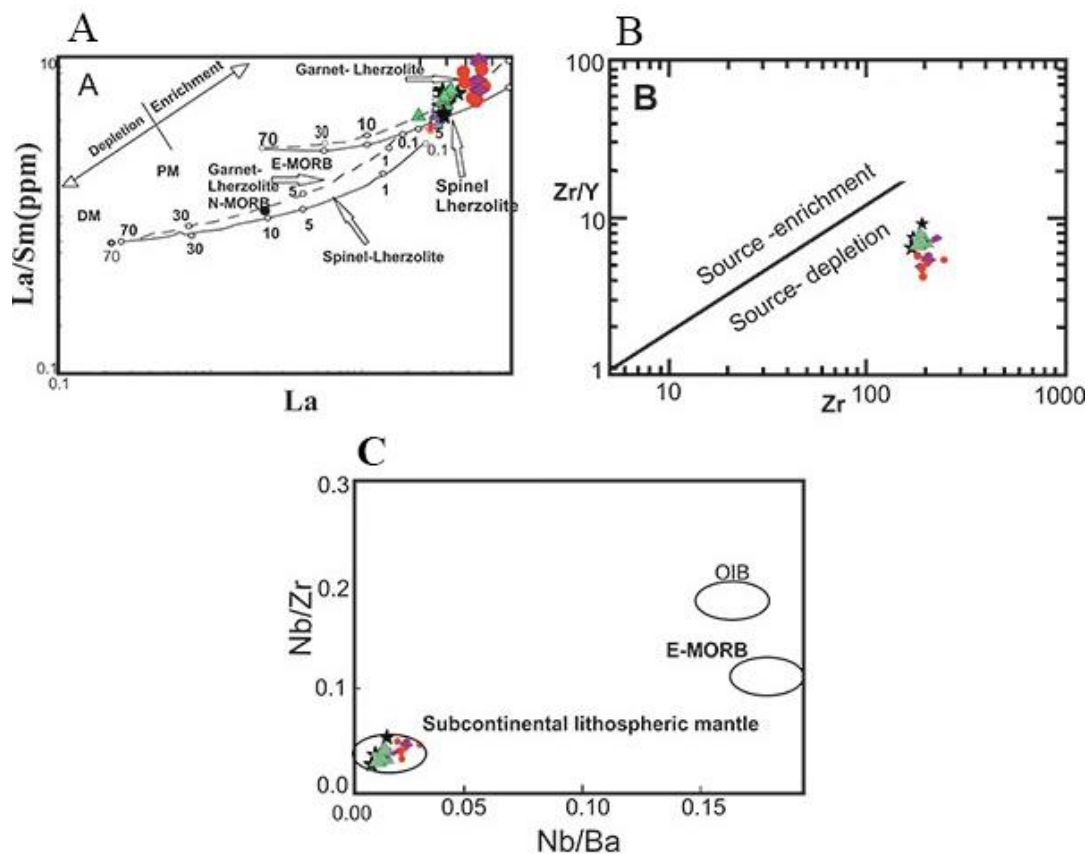


Figure 11. A) diagram La Vs. La/Sm from (33). B) Zr/Y vs Zr diagram to distinguish the rich mantle from the depleted mantle (44). C) The Nb/Zr vs Nb/Ba diagram shows that the region's rocks originate from continental lithospheric mantle (43).

temperature of solidus to decrease (46). At a shallow depth within the Urmia sub-magmatic complex lies the low-velocity zone of the mantle (LVZ) (47- 50). Since the mantle at these depths has been metasomatized by the fluids from the subducted plate, it has suitable conditions for melting (because the fluids lower the solidus and liquidus of the rocks). However, heat is needed to form basaltic magma. As mentioned earlier, the ascent of the deeper asthenosphere causes a relative increase in temperature in the metasomatized mantle. Thus it can lead to the formation of alkaline Goloumak basaltic rocks.

Conclusion

-Neogene volcanic activity in the Goloumak area started with acid units and then continued with alkaline mafic units and calc-alkaline intermediate. These rock units consist of acidic rhyolite and dacite, as well as intermediate andesite, basalt, and trachy-andesite. Mafic igneous rocks are alkaline, and intermediate rocks are calc-alkaline to transition range.

-Volcanic rocks exhibit depletion in Ba, Ti, Nb, and Ta, as well as enrichment in K, Rb, and Th.

-Basaltic rocks were formed by partial melting of the mantle, based on $^{87}\text{Sr}/^{86}\text{Sr}$ and $^{144}\text{Nd}/^{143}\text{Nd}$ isotopic ratios. Samples show relative enrichment of $^{87}\text{Sr}/^{86}\text{Sr}$ in the mantle array on the Sr-Nd isotope correlation diagram.

-Mafic rocks are affected by subduction of lithospheric slab or mantle crust metasomatism, as per the comparison of studied samples in the $^{143}\text{Nd}/^{144}\text{Nd}$ isotope correlation diagram versus $^{87}\text{Sr}/^{86}\text{Sr}$. Based on Sr-Nd geochronological data, the rocks were formed at 12.5 ± 2.0 Ma, corresponding to the Miocene for the basaltic rocks.

-All samples are in a continental arc margin and post-collision volcanic arc. The magma source is from low to intermediate partial melting of the mantle, as indicated by the LREE/HREE ratio of the mafic and intermediate rocks. LREE enrichment is due to low partial melting of mantle source and magma contamination by crust materials. Basalts show a low

melting degree of the mantle for magma formation.

-Depletion of these rocks of HREE in the source shows garnet in genesis. La and Sm abundance in the studied composition is similar to magma derived from the enriched mantle, comprising about 1-5% of lherzolitic garnet.

References

- Alavi, M. Tectonics of the Zagros orogenic belt of Iran: new data and interpretations. *Tectonophysics*. 1994; 220: 211-238
- Nadimi A. Evolution of the Central Iranian Basement. *Gondwana Research*. 2007 Oct 1;12(3):324-33.
- Moghaddam MM, Mirzaei S, Abedi M. New Insights into Interpretation of Aeromagnetic Data for Distribution of Igneous Rocks in Central Iran. *Russian Geology and Geophysics*. 2022 Sep 1;63(9):1061-77.
- Stocklin J, Nabavi MH. Tectonic Map of Iran, 1: 2,500,000, GSI, Tehran-Iran.1973;
- Emami MH. Géologie de la région de Qom-Aran (Iran): Contribution a l'étude dynamique et géochimique du volcanisme Tertiaire de l'I-ran Central. Ph.D. Thèse, Sciences naturelles Univ. Sc. Et Medicale de Grenoble.1981; 489 p.
- Stern RJ, Moghadam HS, Pirouz M, Mooney W. The geodynamic evolution of Iran. *Annual Review of Earth and Planetary Sciences*. 2021 May 30;49:9-36.
- Berberian, M. and King, G. C. P. Towards a paleogeography and Tectonic evolution of Iran. *Canadian Journal of Sciences*.1981; (20) 163–183.
- Shahabpour J, Doorandish M, Abbasnejad A. Mine-drainage water from coal mines of Kerman region, Iran. *Environmental Geology*. 2005 May;47:915-25.
- Ghasemi A, Talbot CJ. A new tectonic scenario for the Sanandaj–Sirjan Zone (Iran). *Journal of Asian Earth Sciences*. 2006 May 1;26(6):683-93.
- Ghasempour MR, Davoudian AR, Shabani N, Moeinzadeh H, Nakashima K. Geochemistry and mineral chemistry of gabbroic rocks from Horjand of Kerman province, Southeast of Iran: Implications for rifting along the northeastern margin of Gondwana. *Journal of Geodynamics*. 2020 Jan 1;133:101675.
- Golestani M, Karimpour MH, Shafaroudi AM, Shahri MR. Geochemistry, U-Pb geochronology, and Sr-Nd isotopes of the Neogene igneous rocks, at the Iju porphyry copper deposit, NW Shahr-e-Babak, Iran. *Ore Geology Reviews*. 2018 Feb 1;93:290-307.
- Dimitrijevic MN, Djockovic I, Cvetic S, Halaviatiz J. Geological map of Rayen 1:1000000 series, sheet 7449, Geological Survey of Iran, Iran. 1979.
- Míková J, Denková P. Modified chromatographic separation scheme for Sr and Nd isotope analysis in geological silicate samples. *J Geosci*. 2007; 52:221–226
- Tanaka T, Togashi S, Kamioka H, Amakawa H, Kagami H, Hamamoto T, et al. JNdi-1: a neodymium isotopic reference in consistency with LaJolla neodymium. *Chemical Geology*. 2000 Aug 1;168(3-4):279-81.
- Shelley D. Igneous and metamorphic rocks under the microscope: classification, textures, microstructures, and mineral preferred orientations. London: Chapman & Hall; 1993.
- Whitney DL, Evans BW. Abbreviations for names of rock-forming minerals. *American mineralogist*. 2010 Jan 1;95(1):185-7.
- Le Bas MJ, Le Maitre RW, Woolley AR. The construction of the total alkali-silica chemical classification of volcanic rocks. *Mineralogy and petrology*. 1992 Mar;46(1):1-22.
- Irvine TN, Baragar WR. A guide to the chemical classification of the common volcanic rocks. *Canadian journal of earth sciences*. 1971 May 1;8(5):523-48.
- Winchester JA, Floyd PA. Geochemical discrimination of different magma series and their differentiation products using immobile elements. *Chemical geology*. 1977 Jan 1;20:325-43.
- Sun SS, McDonough WF. Chemical and isotopic systematics of oceanic basalts: implications for mantle composition and processes. Geological Society, London, Special Publications. 1989;42(1):313-45.
- Le Bas MJ, HR Rollinson. Using Geochemical Data: Evaluation, Presentation, Interpretation. London, 1993. xxvi+ 352 pp. Price£ 24.99 ISBN 0 582 06701 4. *Mineralogical Magazine*. 1994 Sep;58(392):523-.
- Hirschmann M. Origin of the transgressive granophyres from the layered series of the Skaergaard Intrusion, East Greenland. *Journal of Volcanology and Geothermal Research*. 1992 Sep 1;52(1-3):185-207.
- Rollinson HR. Discriminating between tectonic environments using geochemical data. Using geochemical data: evaluation, presentation, interpretation. 1993:171-214.
- Thompson RN. Magmatism of the British Tertiary volcanic province. *Scottish Journal of Geology*. 1982 Feb;18(1):49-107.
- Wandji P, Tchokona Seuwei D, Bardintzeff JM, Bellon H, Platevoet B. Rhyolites of the Mbépit Massif in the Cameroon Volcanic Line: an early extrusive volcanic episode of Eocene age. *Mineralogy and petrology*. 2008 Nov;94:271-86.
- Kurt H, Asan K, Ruffet G. The relationship between collision-related calc-alkaline, and within-plate alkaline volcanism in the Karacadağ Area, Konya-Türkiye, Central Anatolia. *Geochemistry*. 2008 Jun 25;68(2):155-76.
- Wang Y, Fan W, Guo F. Geochemistry of early Mesozoic potassium-rich diorites-granodiorites in southeastern Hunan Province, South China: Petrogenesis and tectonic implications. *Geochemical Journal*. 2003 Aug 20;37(4):427-48.
- Weyer S, Münker C, Mezger K. Nb/Ta, Zr/Hf and REE in the depleted mantle: implications for the differentiation history of the crust–mantle system. *Earth and Planetary Science Letters*. 2003 Jan 10;205(3-4):309-24.
- Zhang HF, Zhang L, Harris N, Jin LL, Yuan H. U–Pb zircon ages, geochemical and isotopic compositions of granitoids in Songpan-Garze fold belt, eastern Tibetan Plateau: constraints on petrogenesis and tectonic evolution of the basement. *Contributions to Mineralogy and Petrology*. 2006 Jul;152:75-88.
- Best, M. G. *Igneous and Metamorphic Petrology*. 2nd Edition. Oxford Blackwell Science. 2003;
- Zindler A, Hart S. *Chemical geodynamics*. Annual review

- of earth and planetary sciences. 1986 May;14(1):493-571.
32. Faure, G. Principles of Isotope Geology. Second Edition, John Wiley & Sons: New York. 1986; 458p.
 33. Aldanmaz, E., Pearce, J. A., Thirlwall, M. F. and Mitchell, J. G. Petrogenetic evolution of late Cenozoic, post-collision volcanism in western Anatolia, Turkey. *Journal of Volcanology and Geothermal Research*. 2000; (102) 67–95.
 34. Ryabchikov, I. D. Babansky, A. D. and Dmitriev, Y. L. Genesis of calc-alkaline magmas: experiment with partial melting of mixed sediments and basalts from the middle America trench, southern Mexico transect. *Initial Reports of Deep Sea Drilling Project*, (66) 669-702 (1982).
 35. Ishizaka K, Carlson RW. Nd-Sr systematics of the Setouchi volcanic rocks, southwest Japan: a clue to the origin of orogenic andesite. *Earth and Planetary Science Letters*. 1983 Sep 1;64(3):327-40.
 36. Pearce J. The role of sub-continental lithosphere in magma genesis at destructive plate margins. *Continental Basalts and Mantle Xenoliths*. 1983.
 37. Keskin M, Pearce JA, Mitchell JG. Volcano-stratigraphy and geochemistry of collision-related volcanism on the Erzurum–Kars Plateau, northeastern Turkey. *Journal of Volcanology and Geothermal Research*. 1998 Oct 1;85(1-4):355-404.
 38. Xiao Y, Niu Y, Li H, Wang H, Liu X, Davidson J. Trace element budgets and (re-) distribution during subduction-zone ultrahigh-pressure metamorphism: Evidence from Western Tianshan, China. *Chemical Geology*. 2014 Feb 4;365:54-68.
 39. Condie KC. High field strength element ratios in Archean basalts: a window to evolving sources of mantle plumes?. *Lithos*. 2005 Feb 1;79(3-4):491-504.
 40. Ellam RM. Lithospheric thickness as a control on basalt geochemistry. *Geology*. 1992 Feb 1;20(2):153-.
 41. Frey FA, Garcia MO, Wise WS, Kennedy A, Gurriet P, Albarede F. The evolution of Mauna Kea volcano, Hawaii: petrogenesis of tholeiitic and alkalic basalts. *Journal of Geophysical Research: Solid Earth*. 1991 Aug 10;96(B9):14347-75.
 42. McKenzie DA, O'Nions RK. Partial melt distributions from inversion of rare earth element concentrations. *Journal of Petrology*. 1991 Oct 1;32(5):1021-91.
 43. Hooper PR, Hawkesworth CJ. Isotopic and geochemical constraints on the origin and evolution of the Columbia River Basalt. *Journal of Petrology*. 1993 Dec 1;34(6):1203-46.
 44. Pearce JA, Norry MJ. Petrogenetic implications of Ti, Zr, Y, and Nb variations in volcanic rocks. *Contributions to Mineralogy and Petrology*. 1979 May;69(1):33-47.
 45. McKenzie DA, Bickle MJ. The volume and composition of melt are generated by the extension of the lithosphere. *Journal of Petrology*. 1988 Jun 1;29(3):625-79.
 46. Gallagher K, Hawkesworth C. Dehydration melting and the generation of continental flood basalts. *Nature*. 1992 Jul 2;358(6381):57-9.
 47. Hearn TM, Ni JF. Pn velocities beneath continental collision zones: the Turkish-Iranian Plateau. *Geophysical Journal International*. 1994 May 1;117(2):273-83.
 48. Maggi A. Structure and evolution of the Alpine-Himalayan belt, PhD thesis, Cambridge University, Cambridge, UK. 2002.
 49. Agard P, Omrani J, Jolivet L, Mouthereau F. Convergence history across Zagros (Iran): constraints from collisional and earlier deformation. *International journal of earth sciences*. 2005 Jul;94:401-19.
 50. Kaviani A, Paul A, Bourova E, Hatzfeld D, Pedersen H, Mokhtari M. A strong seismic velocity contrast in the shallow mantle across the Zagros collision zone (Iran). *Geophysical Journal International*. 2007 Oct 1;171(1):399-410.